RSC Advances

ROYAL SOCIETY OF CHEMISTRY

www.rsc.org/advances

Cite this: DOI: 10.1039/c0xx00000x

www.rsc.org/xxxxxx

ARTICLE TYPE

A novel ferrocene-contained aniline copolymer: its synthesis and electrochemical performance

Chang Su, *[a,b] Lvlv Ji,[a] Lihuan Xu,*[b] Xiaogang Zhu,[a] Huihui He,[a] Yaokang Lv,[a] Mi Ouyang[a] and Cheng Zhang*[a]

Received (in XXX, XXX) Xth XXXXXXXXX 20XX, Accepted Xth XXXXXXXXX 20XX
DOI: 10.1039/b000000x

A novel ferrocene-containing aniline, 6-(2-Amino-phenol-9H-yl)-hexyle ferrocenecarboxylate (AnFc) was synthesized by means of hydrogenation reduction of 6-(2-Nitro-phenol-9H-yl)-hexyle ferrocenecarboxylate (NPFc). Then homopolymer of AnFc (PAnFc), copolymers of aniline and AnFc (P (An-co-AnFc)), polyaniline (PAn) were prepared by chemical oxidative polymerization. The structure, morphology, electrochemical properties of prepared polymers were characterized by fourier transform infrared spectroscopy (FTIR), ultraviolet visible spectroscopy (UV-vis), scanning electron microscopy (SEM), cyclic voltammograms (CV) and galvanostatic charge-discharge testing, respectively. The results demonstrated that the AnFc function monomer and the corresponding polymer derivatives have been synthesized successfully, and the introduction of the novel functional ferrocene-based aniline obviously affected the spectral characteristic, morphology and electrochemical characteristic of the obtained electro-active polymers, as well as its charge migration along polymer backbone. And the charge/discharge tests showed that the P (An-co-AnFc) improved the discharge plateau at the potential rang of about 3.0-4.0 V, with the even acceptable initial discharge specific capacity of 104.9 $mAh \cdot g^{-1}$ for P (An-co-AnFc) (5:1([An]/[AnFc])) (compared with 108.2 $mAh \cdot g^{-1}$ of PAn). Furthermore, P (An-co-AnFc) exhibited an even more improved cycling stability than that of PAn, and after 30 cycles the discharge capacity of P (An-co-AnFc) (3:1([An]/[AnFc]) still maintained 76.3 % of the capacity obtained at the initial cycle.

Introduction

With the development of electronic products, the growing demands for the portable power have recently received widespread attention. Li-ion batteries as one of the widely utilized power technologies have been considered to be the most promising technology in the future, owing to their convenient and good charge-discharge capacity. [1-3] However, the extensive use of this technology is mainly restricted by the positive electrode, which usually shows a much lower capacity than that of the negative one. The current Li-ion battery cathode materials are mostly transition-metal materials (such as $LiCoO_2$, $LiMn_2O_4$, $LiFePO_4$ and V_2O_5, etc.), which, however, have the series of drawbacks, such as the limited theoretical capacities, the limited mineral resources and waste treatment process. [4-7] In addition, the high energy demand and CO_2 emissions during the production process also limits the development of these materials as the cathodes of Li-ion batteries in the future. [8] Hence, there exists an increasing desire to exploit novel materials for Li-ion batteries by many groups. As an alternative, the application of organic materials as cathode materials in Li-ion batteries have been significant investigated because of their easy preparation and high theory energy density, as well as their designability as the flexible Li-ion batteries, although they have some well-known problems, such as relatively poor performances in practical capacity and stability. So far, various organic electroactive materials have been explored as positive-electrode materials, mainly including electroactive conducting polymers, [9, 10] organosulfur polymers, [11] nitroxide radical tetramethylpiperidine-N-oxyl (TEMPO)-based polymers, [12, 13] pendant-type polymer based on ferrocene and carbazole, [14, 15] aromatic carbonyl derivatives and quinine-based materials, etc. [16]

Among them, conducting polymers (such as polyacetylene (PAc), [17] polythiophene (PTh), [18, 19] polypyrrole (PPy) [20, 21] and polyaniline (PAn), [22] etc.) and their derivatives appear to be the most probable candidates due to their high electronic conductivity and reversible redox characteristics. Polyaniline (PAn) is a promising candidate for the electrode materials because of its environmental stability, light weight, shape flexibility and low production cost which satisfy the most of the basic requirements of Li-ion battery cathode materials. [23] PAn firstly served as the cathode material of Li-ion battery in 1969, which has the highest specific energy (539.2 $Wh \cdot kg^{-1}$) among the current conducting polymers by the research of MacDiamid. [24] However, PAn has several disadvantages, such as the sloping charge-discharge plateau curves at 2.5-4.1 V and the poor cycling stability, which limit its application in Li-ion battery. [25]

As a typical organo-metallic compound, ferrocene is promising as the active electrode material, because of its air stability, excellent electrochemical response, solvent independent redox behavior, and so on. [26-28] To improve the stability of ferrocene molecular applied as electrode material, it has been designed to form the stable polymers carrying ferrocene moieties, such as poly(vinylferrocene), poly(ethynylferrocene) and poly(ferrocene). When applied as cathode-active materials for the organic cathode

of lithium ion batteries, the ferrocene-contained polymers exhibit the promising electrochemical properties, such as quick charge/discharge ability, high power density, and flat and stable voltage plateaus (~3.4V). [14] However, above ferrocene contained polymers are derivatives of conventional plastics, which are insulator, resulting in the electron migration among the polymer limited. As a result, a very large amount of conducting agents (such as carbon black, graphite, graphene and carbon fibers), even up to 60-80 wt% of the total electrode, is required in the fabrication of the composite electrode, in order to improve the long-range conductivity and the utilization rate of ferrocene-contained the electro-active polymers. This leads to the actual redox capacity of the composite electrode to decrease seriously, and the extensive studies to use them as active materials for batteries are impeded. Because the intrinsic conductivity for most of ferrocene-contained polymers are rather low due to the insular polymer backbone, so a combination of the electroactive ferrocene with a conductive polymer is regarded as an effective way to produce a new ferrocene-contained polymer with the improved the electron migration. In light of these considerations, we anticipate to use PAn as the main chain to prepare the ferrocene-containing PAn derivates, aiming to prepare a novel electroactive material for the cathode of the lithium ion battery.

In this article, a novel ferrocene-contained aniline monomer was synthesized, and the homopolymer of AnFc (PAnFc) and the corresponding copolymers An and AnFc (P (An-co-AnFc)) with different ratio of An/AnFc were then prepared by chemical oxidation polymerization. The molecular structure, morphology, electron migration characteristics and the electrochemical performance of the polymers as a cathode material were evaluated, respectively. It was found that introduction of AnFc functional monomer in polymer demonstrated an improved PAn's discharge plateau curves and an acceptable initial specific capacity, which makes it a promising reference for designing and preparing the novel organic cathode with the high cell performance.

Experimental

Materials

6-Chloro-hexan-1-ol (98 %), Ferrocenecarboxylic acid (99 %) and Aniline (99.98 %) were purchased from Aladdin-Reagent Co. 2-Nitro-phenol (AR) was purchased from Energy Chemical Reagent Co. Pt/C catalyst was purchased from Johnson Matthey Catalyst Co. All other reagents were received as analytical grade and used without further purification.

Material synthesis

Synthesis of AnFc monomer

The synthesis process of the monomer (AnFc) was shown in Scheme 1.

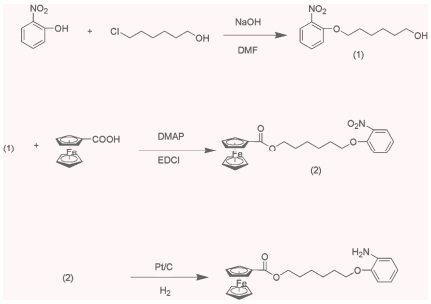

Scheme 1. The synthesis route to AnFc

Synthesis of 6-(2-Nitro-phenoxy)-hexan-1-ol (NPHO): 2-Nitro-phenol (2.78 g, 0.02 mol), 6-Chloro-hexan-1-ol (3.28 g, 0.024 mol), sodium hydroxide (1.2 g, 0.03 mol) and 40 ml N,N-Dimethylformamide (DMF) were mixed in a pre-dried flask. The mixture was heated reflux (60 ℃) for 72 h until turning to vivid orange-red. After cooled, the resulting solution was then extracted with CH_2Cl_2, the organic fraction was washed with saturated brine for three times and then dried by anhydrous $MgSO_4$. The obtained 6-(2-Nitro-phenoxy)-hexan-1-ol was isolated by column chromatography (silica gel, petroleum ether/ethylacetate 50:1) with 78 % yield as reseda liquid. MS (EI): calculated for $C_{12}H_{17}NO_4$ m/z: 239.12, found m/z: 239.8.1H NMR (500 MHz, $CDCl_3$) δ: 7.82 (dd, J=8.1, 1.7 Hz, 1H), 7.51 (ddd, J=8.9, 7.5, 1.6 Hz, 1H), 7.10-7.04 (m, 1H), 7.03-6.98 (m, 1H), 4.11 (t, J=6.3 Hz, 2H), 3.67 (t, J=6.5 Hz, 2H), 1.89-1.82 (m, 2H), 1.65-1.58 (m, 2H), 1.56-1.52 (m, 3H), 1.45 (tdd, J=8.7, 6.0, 2.9 Hz, 2H).

Synthesis of 6-(2-Nitro-phenol-9H-yl)-hexyle Ferrocenecarboxylate (NPFc): 6-(2-Nitro-phenoxy)-hexan-1-ol (3.59 g, 0.015 mol) and ferrocenecarboxylic acid (4.14 g, 0.018 mol) were dissolved in 40 ml dichloromethane in a pre-dried flask, then 1-(3-Dimethylaminopropyl)-3-ethylcarbodiimide hydrochloride (3.45 g, 0.018 mol) as dehydrating agent and 4-dimethylaminopyridine (0.92 g, 0.0075 mol) were added as acylating catalyst, and stirring for 24 h at room temperature. The reaction mixture was extracted with CH_2Cl_2, the organic fraction was washed with saturated brine for three times and then dried by anhydrous $MgSO_4$. The ester was purified by column chromatography using silica gel and petroleum ether/ethyl acetate afforded the title compound as reddish-brown solid. MS (EI): calculated for $C_{23}H_{25}FeNO_5$ m/z: 451.11, found m/z: 450.8. 1H NMR (500 MHz, CDC_{l3}) δ: 7.82 (dd, J=8.1, 1.5 Hz, 1H), 7.53-7.48 (m, 1H), 7.07 (d, J=8.4 Hz, 1H), 7.04-6.98 (m, 1H), 4.81 (t, J=1.7 Hz, 2H), 4.42-4.36 (m, 2H), 4.24 (q, J=6.5 Hz, 2H), 4.20 (d, J=4.2 Hz, 5H), 4.12 (t, J=6.3 Hz, 2H), 1.92-1.85 (m, 2H), 1.81-1.74 (m, 2H), 1.60 (dt, J=10.9, 7.0 Hz, 2H), 1.56-1.48 (m, 2H).

Synthesis of 6-(2-Amino-phenol-9H-yl)-hexyle Ferrocenecarboxylate (AnFc): [29] Liquid phase hydrogenation of 6-(2-Nitro-phenol-9H-yl)-hexyle and ferrocenecarboxylate was carried out in a 500mL stainless steel autoclave with a magnetic stirring bar. The reaction system included 4 g 6-(2-Nitro-phenol-9H-yl)-hexyle Ferrocenecarboxylate, 150 mL of methanol, and 0.2 g of Pt/C catalyst. In order to exclude the inside air, the autoclave was purged with hydrogen 6 times, and then raised the pressure to 4.0 MPa (hydrogen) and then raised the temperature to 70 ℃. Not untill temperature reached a steady state, the stirring started at 800 rpm and the pressure was maintained constant at 4.0 MPa. After a given period of reaction time or after no hydrogen uptake was observed, the reactor was cooled down to room temperature and the pressure in the reactor was released. The product was obtained by filtered out the Pt/C catalyst and evaporated the methanol. MS (EI): calculated for $C_{23}H_{27}FeNO_3$ m/z: 421.13, found m/z: 421.3.1H NMR (500 MHz, CDC_{l3}) δ: 6.82-6.72 (m, 4H), 4.83-4.81 (m, 2H), 4.40 (t, J=1.9 Hz, 2H), 4.24 (t, J=6.6 Hz, 2H), 4.21 (s, 5H), 4.03 (t, J=6.4 Hz, 2H), 1.92-1.84 (m, 2H), 1.82-1.74 (m, 2H), 1.62-1.51 (m, 4H).

Chemical polymerization of PAn, PAnFc and P(An-co-AnFc)

All of PAn, PAnFc and P(An-co-AnFc) were prepared by the same method. An and/or AnFc (mass ratios of [An]/[AnFc]: 0:1, 2:1, 3:1, 5:1, 1:0) were dispersed in a 0.5 M camphorsulfonic acid (CSA) solution. Ammonium persulfate (APS) in a CSA solution (APS/[An+AnFc] molar ratio=1.2:1) was then slowly added dropwise. The mixture was stirred in a nitrogen atmosphere at 3-5 ℃ for 24 h. The precipitates were filtered and washed with

deionized water and ethanol. The polymers were dried under vacuum at 60 ℃.

Material characterization

FT-IR spectra were obtained on a Nicolet 6700 spectrometer (Thermo Fisher Nicolet, USA) with KBr pellets. UV-vis spectra were recorded on a Varian Cary 100 UV-vis spectrophotometer (Varian, USA). 1H NMR spectra of the compounds were recorded on a Brucker AVANCE III 500 MHz spectrometer (Bruker, Switzer-land) using $CDCl_3$ and DMSO-d_6. The mass spectrometry (MS) analysis was measured on a GCT premier spectrometer (Waters, USA) using the electron impact (EI^+) mass spectra technique. Scanning electron microscopy (SEM) measurements were taken using a Hitachi S-4800 scanning electron microscope (Hitachi, Japan).

Electrochemical measurements

For cathode characterization, CR2032-type coin cell was used and assembled in an argon-filled glove box. The cathode were prepared by coating a mixture containing 50% as prepared polymers, 40% acetylene black, 10 % PVDF binder on circular Al current collector foils, followed by dried at 60 ℃ for 10 h. After that, the cells were assembled with lithium foil as the anode, the prepared electrodes as cathode and 1M $LiPF_6$ dissolved in ethylene carbonate (EC) and dimethyl carbonate (DMC) (EC/DMC = 1:1, v/v) as the electrolyte. The charge-discharge measurements were carried out on a LAND CT2001 A in the voltage range of 2.5-4.2V versus Li/Li^+, using a constant current density at room temperature. The cyclic voltammograms (CV) tests were performed with CHI 660E electrochemical working station in 0.1M $LiClO_4/CH_3CN$ versus Ag/AgCl at a scan rate of 50 $mV.s^{-1}$.

Results and discussion

Synthesis and Characterization of AnFc

The chemical structure of AnFc was confirmed by 1H NMR and mass spectrometry (MS), respectively. Therein, NPHO was synthesized firstly through an etherification reaction of 2-Nitro-phenol and 6-Chloro-hexan-1-ol in DMF solvent, then attaching a ferrocene moiety on it to form NPFc. Finally, AnFc was synthesized by reducing the nitro group on NPFc intermediate to an amino group with Pt/C as catalysis and H_2 as reductant in the stainless steel autoclave.

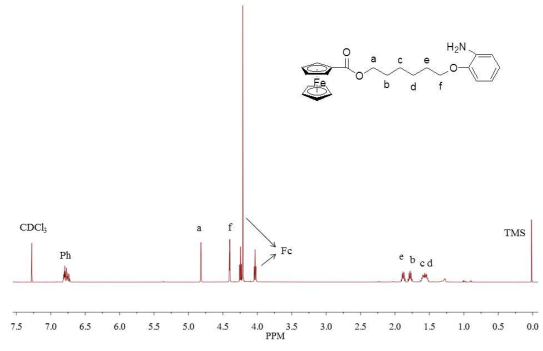

Fig. 1. ^{1}H NMR spectrum of AnFc in $CDCl_3$.

The ^{1}H NMR spectrum of AnFc was shown in Fig. 1.The protons of the methene groups next to oxygen in AnFc exhibit two peaks at 4.82 and 4.40 ppm, respectively. And the proton peaks for other methene group locate between 1.52 and 1.91 ppm, while the peaks between 4.02 and 4.26 ppm are confirmed to be the protons of the ferrocene moiety. What's more, the peaks between 6.72 and 6.82 ppm are proved to be the protons of the phenyl ring. However, the peak of the amino protons has not appeared, possibly caused by the reactive hydrogen (the fast exchange between amino protons and deuterons from $CDCl_3$ solution).

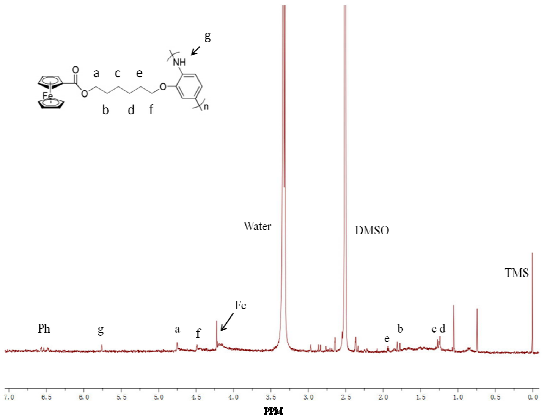

Fig. 2. 1H NMR spectrum of PAnFc in DMSO-d_6.

The ^{1}H NMR spectrum of PAnFc was also measured with DMSO-d_6 as solvent, as shown in Fig. 2. it can be seen that the splitting peaks at 6.4-6.6 ppm in Figure are assigned to the aromatic proton resonance of PAnFc. The multiplet peaks at 4.0-4.3 ppm are confirmed to be the protons of ferrocene moiety. What's more, the peak at 4.75 and 4.49 ppm characterize the protons of the methene groups next to oxygen in PAnFc. Furthermore, the proton peaks for other methene group locate between 1.20 and 1.95 ppm, while the peak at 5.76 ppm is caused by NH resonance.[30, 31]

Material characterization

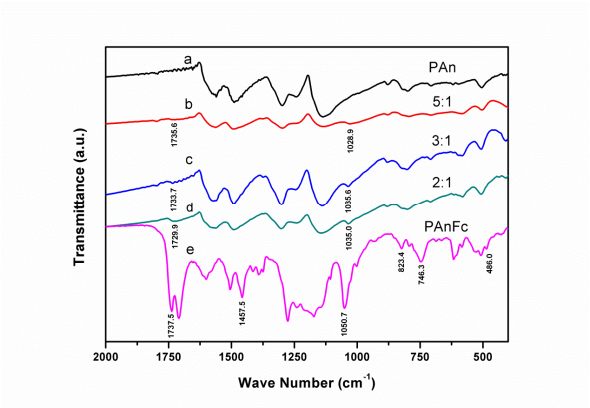

Fig. 3. FTIR spectrum of the (a) PAn, (b) P (An-co-AnFc) (5:1), (c) P (An-co-AnFc) (3:1), P (An-co-AnFc) (2:1) and PAnFc samples.

Fig.3 showed the FT-IR spectra of PAnFc, P (An-co-AnFc) and PAn, respectively. The main characteristic peaks for PAn are shown, in which the absorption peaks at 1560-1580 cm^{-1} and 1485-1495 cm^{-1} are attributed to the C=C stretching bands of the quinoid and benzeniod rings respectively and the absorption peaks at 1130-1150 cm^{-1} is due to the C-N stretching (as shown in Fig. 3 (a)). In Fig. 3 (e), the similar characteristic bands of PAn are presented in PAnFc, while the characteristic peaks for the

C=C stretching band of the quinoid obviously red-shift to the high wavenumbers, which can be regarded as the contribution of the electron donating effect of the alkoxy group on the benzene ring. In addition, some new bands can be observed clearly in the spectrum of PAnFc, in which the absorption peak of 1737.5 cm^{-1} is the stretching of C=O (ester carbonyl) and the absorption peak of 1457.5 cm^{-1} is attributed to the -CH_2 stretching vibration. And the absorption peaks at 1050.7, 823.4 and 486.0 cm^{-1} are due to the mono-substituted ferrocene. For the copolymers-P (An-co-AnFc) with the different feeding ratio of AnFc and An, the main bands are similar to those of the PAn. Furthermore, there are two new peaks observed in the copolymers, in which the absorption of 1729-1736 cm^{-1} is the stretching of C=O (ester carbonyl) and the absorption at 1028-1036 cm^{-1} is still due to the ferrocene units. It can also be observed that the intensity of both new peaks increase with the increasing ratio of AnFc/An. All those indicate that both aniline and ferrocene moieties are included in polymers and the P (An-co-AnFc) copolymers and PAnFc polymers have been successfully prepared.

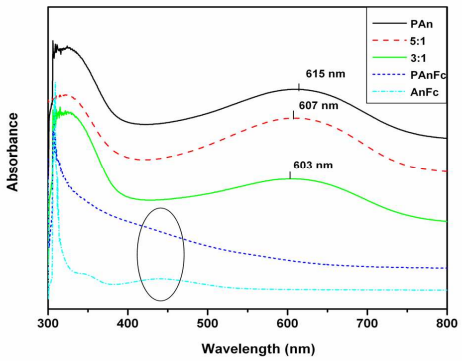

Fig. 4. UV-vis spectra of PAn, P (An-co-AnFc) (5:1), P (An-co-AnFc) (3:1), PAnFc and AnFc.

The UV-vis spectra (normalized absorbance) were further measured to explore on the characteristics of the emeraldine-base form of polymers (P (An-co-AnFc) (3:1), P (An-co-AnFc) (5:1), PAn and PAnFc) (de-doped state polymers) and monomer (AnFc) in DMF. As can be seen, PAn in the emeraldine-base state shows typical absorption peaks at 319 nm (π-π^* transition of the aniline unit of emeraldine type) and 603 nm (n-π^* transition in the quinine imine unit of the basic structure). [32, 33] For PAnFc, both the stronger absorption peaks at ~320 nm and the side-peak at ~470 nm are corresponding to the π-π^* electron transition of the ferrocene moieties, which is in accrod with the measured results of AnFc monomer in UV-Vis spcetra, in which the correspondingly characteristic peaks occur almost in the similar positions. Specially, there are not obvious characteristic peaks of PAn being observed for PAnFc, which is due to that the large steric effect of the bulky AnFc groups seriously breaks the conjugated structure of the neighbour An unites in the PAn backbone, resluting in the electron delocalization ineffective and the corresponding disappearance of the characteristic peaks of PAn. For copolymers, the emeraldine-base form of P (An-co-AnFc) exhibits the similar spectra to that of PAn. And the absorption peaks at ~ 320 nm are still attributed to the π-π^* transition of the aniline unit of PAn backbone, while a hypsochromic in the absorbance for n-π^* transition in the quinine imine unit of the basic structure are noticed for the copolymers with the increase of the feeding ratio of AnFc/An, as compared with PAn. It indicates that the electron delocalization in the PAn backbone is reduced, causing by the increasing content of the bulky AnFc groups into PAn backbone with the increase of the feeding ratio of AnFc/An as supported by MALDI-TOF analysis (as shown in the supporting information), which will lead to seriously torsion for the obtained polymer chain and the destruction of the conjugated structure of P (An-co-AnFc). As a result, the electron delocalization along the copolymer backbone becomes ineffective and a hypsochromic shift of the UV-Vis spectra characteristic for P (An-co-AnFc) copolymers occurs.

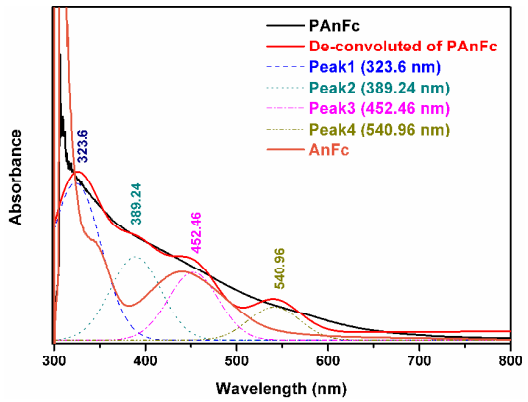

Fig. 5. De-convoluted analysis of UV-Vis spectra of PAnFc.

PeakFit has been used to de-convolute the results of UV-vis spectrum of PAnFc, which was shown in the Fig. 5. Compared to the original curve of UV-vis spectra of PAnFc, after the de-convolution, four obvious peaks appear at 323.6, 389.24, 452.46 and 540.96 nm, respectively, in which the peaks at 323.6, 389.24 and 452.46 nm is in accord to the characteristics of AnFc moieties in the PAnFc and the peak at 540.96 nm is due to the n-π^* transition in the quinine imine unit of PAnFc. Furthermore, it can be observed that the characteristic absorption peaks of AnFc for PAnFc are obviously bathochromic shift compared to that of AnFc monomer which is at 315.2, 358.8 and 446.2 nm, respectively. It is due to the enhanced conjugation after polymerization, which leads to the improved electron delocalization in the PAnFc. While the characteristic peak for the n-π^* transition of the quinine imine unit of PAnFc backbone (540.96 nm) is obviously the hypsochromic shift compared to that of both PAn and P (An-co-AnFc), indicating that the electron delocalization in the PAn backbone is reduced, caused by the introduction of AnFc pendant which causes seriously torsion for the obtained polymer chain and destructs the conjugated structure of PAn. All the results are in accordance with our hypothesis.

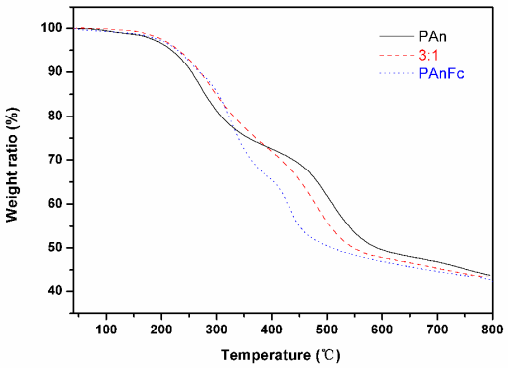

Fig. 6. TG of PAn, P (An-co-AnFc) (3:1), PAnFc.

The thermal stability of PAnFc, P (An-co-AnFc) (3:1) and PAn has been measured, as shown in the Fig. 6. As can be seen, the mass loss of the polymers over the temperature range between 40 to 200°C is attributed to the loss of the residual water and solvent molecular. A sharp mass transition occurring at about 200-350°C is owing to the degradation of doped acid CSA in the polymers matrix. When the temperature is over 350 °C, the weight loss for three polymers with the increasing temperature is due to the degradation and the carbonation process of the polymer skeleton. Form figure, it can be seen that PAnFc as well its copolymer has the larger weight loss at high temperature than that of Pan which exhibit the better thermal-stability. This is considerate due to the catalysis function of Fe element in the ferrocene-contained polymers which improves the degradation and the carbonation process of the polymer skeleton during the thermal-treatment process. Furthermore, the electrical conductivity of the polymers has also been measured using the four probe technology, in which PAnFc, P (An-co-AnFc) (3:1) and PAn have 2.1×10^{-6} S/cm, 5.7×10^{-3} S/cm and 1.9 S/cm, respectively. The reduced electrical conductivity for the ferrocene-contained polyaniline derivatives compared to PAn can still be attributed to the large steric effect of the bulky AnFc, which deduces the conjugated structure of the polymer chain and the electron transfer along the polymer.

Fig. 7 showed the SEM images of PAn, PAnFc, P (An-co-AnFc) (2:1), P (An-co-AnFc) (3:1) and P (An-co-AnFc) (5:1), respectively. As can be seen, PAn particles with aggregation structure are obviously observed in Fig. 7(a). Comparatively, with the introduction of the ferrocene-based moiety into PAn, the morphologies of PAnFc and copolymers change obviously from that of PAn. And PAnFc sample exhibits the high identity particle-like structure with the nanosizes from 40 nm to 100 nm (shown in Fig. 7 (b)). For the samples of P (An-co-AnFc) (5:1), P (An-co-AnFc) (3:1) and P (An-co-AnFc) (2:1), the copolymers show the more porous and looser morphologies with the increase of ferrocene-based moiety into copolymers. The different morphology can be attributed to the introduction of ferrocene-contained functional monomer, which leads to the different polymer molecular structure and then the different molecular aggregation behavior, as well as the resulted morphology of polymers. The porous morphology and the loose structure are in favor of the contact of electrode-active material and electrolyte, thus providing the sufficient ionic channels for the redox reactions of the electroactive electrode during the charge/discharge process, which is very important for preparing a good cathode material for Li-ion batteries. BET analysis of the polymers have also be measured, which is 1.2 m^2/g for PAn, 2.7 m^2/g for PAnFc, 4.0 m^2/g for P (An-co-AnFc) (2:1), 4.6 m^2/g for P (An-co-AnFc) (3:1) and 2.2 m^2/g for P (An-co-AnFc) (5:1), respectively. The results indicate the introduction of AnFc units in copolymer increases the specific surface, which is in accord to SEM analysis before.

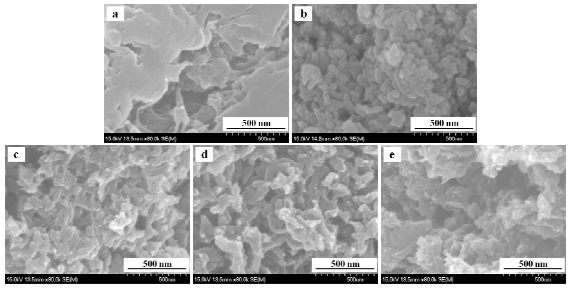

Fig. 7. SEM images of powder samples (a) PAn, (b) PAnFc, (c) P (An-co-AnFc) (2:1), (d) P (An-co-AnFc) (3:1) and (e) P (An-co-AnFc) (5:1)

Electrochemical performance

Fig. 8 showed the cyclic voltammetry (CV) profiles of the PAn, P (An-co-AnFc) (5:1), P (An-co-AnFc) (3:1), P (An-co-AnFc) (2:1) and PAnFc, measured in 0.1 M lithium perchlorate/acetonitrile solution. As shown in the figure, PAn exhibits one pair of broad redox peaks at ~0.81 and ~0.4 V vs. Ag/AgCl, which are corresponding to the oxidation (Li^+ or ClO_4^- doping) and the reduction (Li^+ or ClO_4^-dedoping) process of PAn. For the electrode of PAnFc, it shows one couple of obvious redox peaks with the similar peak shape at 0.50 and 0.24V vs. Ag/AgCl, which is assigned to the charge-discharge reaction of the redox couple of ferrocene-based moiety (Fe^{2+}/Fe^{3+} couple). However, there are no the redox peaks of the PAn backbone in PAnFc being observed, which can be ascribed to that the large steric effect of side-chain pendants impedes the conjugation of the conducting PAn backbone and the resulted redox process of PAn during the charge-discharge process, leading to the disappearing of characteristic peaks of PAn. For the copolymers, with the increase of the ferrocene-contained aniline content to copolymer, the redox peak intensity for the redox couple of ferrocene-based moiety in low potential becomes strong gradually, while the intensity for PAn in the high potential one decreases, correspondingly. Meanwhile, the redox peak couples shift to high potential with the increase of the content ferrocene-contained aniline in copolymer, and specially, for P (An-co-AnFc) (2:1) sample, a pair of board and overlapped peaks is presented in CV curve. The results indicate that ferrocene-contained aniline has been successfully included in copolymer, and the introduced functional monomer affects the corresponding electrochemical characteristics of PAn.

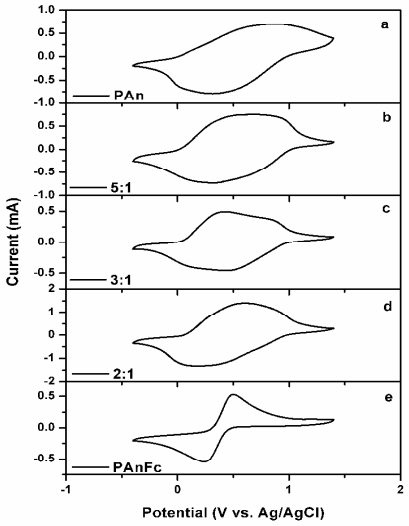

Fig.8. Cyclic voltammograms (CV) of (a) PAn, (b) P (An-co-AnFc) (5:1), (c) P (An-co-AnFc) (3:1), (d) P (An-co-AnFc) (2:1) and (e) PAnFc in 0.1 M $LiClO_4/CH_3CN$ versus Ag/AgCl at the scan rate of 50 $mV.s^{-1}$.

Charge-discharge performance

The charge-discharge behaviors of the as-prepared polymers as cathode of lithium batteries had been further investigated by simiulated lithium ion half-cell method. The initial charge-discharge profiles of the polymers at 20 $mA.g^{-1}$ between 2.5 and 4.2 V were shown in Fig. 9. As we can see from Fig. 9 (a), the

PAnFc exhibits a 35.5 mAh.g^{-1} capacity at the initial cycle, which is 55.78 % of the theoretical capacity (63.64 mAh.g^{-1}) (considering that PAn has no contribution to the total capacity, due to having no redox peaks occurring in the CV curve of Fig. 8(e)). Particularly, a flat voltage plateaus is obviously observed in the charge-discharge curves of the PAnFc, which is assigned to the redox characteristics of organic-metallic ferrocene (Fe^{2+}/Fe^{3+} couple). Comparatively, PAn shows an initial discharge capacity of 108.2 mAh.g^{-1} at initial cycle, and has no obvious discharge platform at all, which is corresponding to the conventional reported result. In addition, the initial discharge capacity of P (An-co-AnFc) (2:1), P (An-co-AnFc) (3:1) and P (An-co-AnFc) (5:1) are 61.5, 88.2 and 104.9 mAh.g^{-1} respectively, in which the discharge capacity increases accordingly with the increase proportion of aniline-based moiety in the copolymers. That is because PAn has a relatively higher theoretical specific capacity than PAnFc. However, it is worth noting that copolymers present the improved sloping plateaus and a more steady discharge voltage plateau than that of PAn, which can be attributed to the Fe^{2+}/Fe^{3+} redox couple of the ferrocene group which possesses a stable voltage plateaus near 3.4 V during the charge/discharge process.

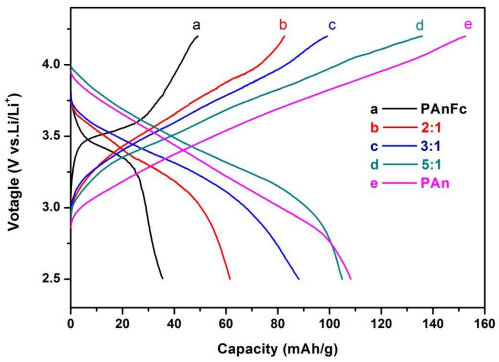

Fig. 9. Initial charge/discharge profiles of (a) PAnFc, (b) P (An-co-AnFc) (2:1), (c) P (An-co-AnFc) (3:1), (d) P (An-co-AnFc) (5:1) and (e) PAn electrodes material at a constant current of 20 mA.g^{-1} between 2.5 and 4.2 V in $LiPF_6$ EC/DMC (v/v, 1:1) electrolyte versus Li/Li^+.

The cycling stability of the electroactive polymers was also studied, and PAn, P (An-co-AnFc) (3:1) and PAnFc were chosen as the aim polymer for this evaluation (shown in Fig. 10). As depicted in Figure, PAnFc exhibits a significant obvious good cycling stability, and after 30th cycles, the discharge capacity changes from 35.5 mAh.g^{-1} to 32.7 mAh.g^{-1} with only about 7.9 % loss of the initial capacity. For the PAn, it exhibits a serious capacity decay in the initial 10 cycles, while the capacity of the following cycles maintains relatively stable. As the ferrocene-contained aniline is introduced in PAn, it is found that the specific capacity of P (An-co-AnFc) (3:1) changes from 88.2 mAh.g^{-1} to 67.3 mAh.g^{-1} with about 23.7 % capacity degeneration, in which the cycling stability is obviously improved compared to that of PAn, specially in the initial several cycles, although accompanying some capacity fluctuation during the cycling process. The results reveal that introduction of AnFc into polymer can improve the cycling stability in some degree, which is ascribed to the excellent electrochemical stability of ferrocene and the improved polymer morphologies.

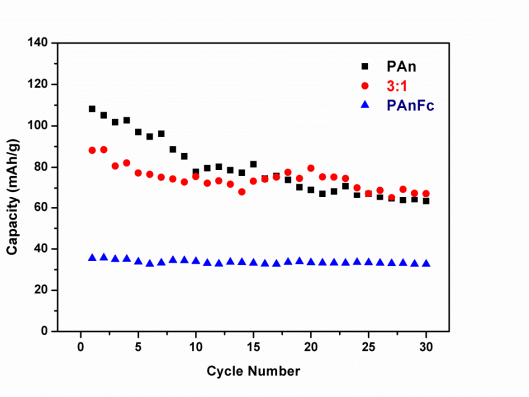

Fig. 10. The cycling performance of PAn, P (An-co-AnFc) (3:1) and PAnFc

Conclusions

A novel aniline derivative (AnFc) with the ferrocene-based moiety had been synthesized successfully. And the series of the conducting homopolymer and copolymers based on aniline and AnFc were obtained by chemical oxidation polymerization. The characteristics of FTIR, UV-Vis and CV indicated that AnFc functional unit has been successfully introduced in the polymer. And the novel AnFc monomer in the PAn-based polymers impeded the charger migration along the PAn backbone to some extent (as the observed hypsochromic in the absorbance for n-π^* transition in the quinine imine unit of PAn from UV-Vis and FIRT) and made the CV curves exhibiting the characteristics of both PAn and ferrocene together. SEM measurement demonstrated that the agglomeration of PAn was greatly improved by the introduction of ferrocene-basd moiety and the smaller particles with the loosing structure were presented. And the charge/discharge tests showed that the P (An-co-AnFc) improved the discharge plateau at the potential rang of about 3.0-4.0 V, with the even acceptable initial discharge specific capacity of 104.9 mAh·g^{-1} for P (An-co-AnFc) (5:1) (compared with 108.2 mAh·g^{-1} of PAn), while PAnFc presented a initial capacity of 35.5 mAh.g^{-1} because of relatively low theory capacity of PAnFc, Furthermore, P (An-co-AnFc) exhibited an even more improved cycling stability than PAn, and after 30 cycles the discharge capacity of P (An-co-AnFc) (3:1) still maintained 76.3 % of the capacity obtained at the initial cycle.

Acknowledgements

The authors thank the National Natural Science Foundation of China (NSFC, No. 51003095) and Research on Public Welfare Technology Application Projects of Zhejiang Province, China (2010C31121) for financial support. This work also was supported by the analysis and testing foundation of Zhejiang University of Technology.

Notes and references

[a] State Key Laboratory Breeding Base for Green Chemistry Synthesis Technology, College of Chemical Engineering, Zhejiang University of Technology, Chaowang Road 18#, Hangzhou, 310014, P. R China
[b] College of Chemical Engineering, Shenyang University of Chemical Technology, Shenyang, 110142, P. R. China.
*Corresponding author. Tel.: +86-24-89383902; Fax: +24-89383902.
E-mail address: suchang123@hotmail.com (Chang Su); xulihuanss@163.com (Lihuan Xu); czhang@zjut.edu.cn (Cheng Zhang)

1 Y. Hu, X. Sun, *J. Mater. Chem. A*. 2014, **2**, 10712.

2 A.Yoshino, *Angew. Chem. Int. Ed.,* 2012, **51(24)**: 5798.

3 M. Armand, J. M. Tarascon, *Nature.* 2008, **451**, 652.

4 B. Xu, D. Qian, Z. Wang, Y. S. Meng, *Mater. Sci. Eng.* 2012, **R 73**, 51.

5 C. Masquelier, L. Croguennec, *Chem. Rev.* 2013, **113**, 6552.

6 A. Kraytsberg, Y. Ein-Eli, *Adv. Energy. Mater.* 2012, **2**, 922.

7 P. G. Bruce, B. Scrosati, J. M. Tarascon, *Angew. Chem. Int. Ed.* 2008, **47**, 2930.

8 H. Y. Chen, M. Armand, G. Demailly, F. Dolhem, P. Poizot, J. M. Tarascon, *ChemSusChem.*. 2008, **1**, 348.

9 L. Yanliang, T. Zhanliang, C. Jun, *Adv. Energy. Mater.* 2012, **2**, 742.

10 K. S. Park, S. B. Schougaard, J. B. Goodenough, *Adv. Mater.* 2007, **19**, 848.

11 Y. X. Yin, S. Xin, Y. G. Guo, L. J. Wan, *Angew. Chem. Int. Ed.* 2013, **52**, 2-18.

12 T. Suga, H. Konishi, H. Nishide, *Chem. Commun.* 2007, **17**, 1730.

13 J. Qiu, T. Katsumata, M. Satoh, J. Wada, T. Masuda, *Polymer.* 2009, **50 (2)**, 391.

14 K. Tamura, N. Akutagawa, M. Satoh, J. Wada, T. Masuda, *Macromol.Rapid.Commun.* 2008, **29**, 1944.

15 M. Yao, H. Senoh, T. Sakai, T. Kiyobayashi, *J. Power. Sources.* 2012, **202**, 364.

16 M. Yao, H. Senoh, S. Yamazaki, Z. Siroma, T. Sakai, K. Yasuda, *J. Power. Sources.* 2010, **195**, 8336.

17 H. Shirakawa, E. J. Louis, A. G.MacDiarmid, *Chem. Commun,* 1977, 578.

18 A. Laforgue, P. Simon, C. Sarrazin, J.F. Fauvarque, *J. Power. Sources.* 1999, **80,** 142.

19 C. C. Changa, L. J. Her, J. L. Hong, *Electrochim. Acta.* 2005, **50**, 4461.

20 T. Osaka, T. Momma, K. Nishimura, S. Kakuda, T. Ishii, *J. Electrochem. Soc.* 1994, **141**, 1994.

21 P. Novák, W. Vielstich, *J. Electrochem. Soc.* 1900, **137**, 1681.

22 J. Manuel, J. K. Kim, A. Matic, P. Jacobsson, G. S. Chauhan, J. K. Ha, K. K. Cho, J. H. Ahn, *Mater. Res. Bull.* 2012, **47**, 2815.

23 J. Zhang, D. Shan, S. Mu, *J. Power. Sources.* 2006, **161**, 685.

24 A. G. MacDiarmid, J. C. Ching, J. C. Richter, A. J. Epstein, *Synth. Met.* 1987, **18(2)**, 285.

25 K. S. Ryu, K. M. Kim, *J. Power. Sources.* 2007, **165**, 420.

26 T. Saji, Y. Maruyama, S. Aoyagui, *J. Electroanal. Chem.* 1978, **86**, 219.

27 J. Irena, B. Stanley, J. Angela, H. A. Robert, *J. Solid. State. Electrochem.* 2004, **8**, 403.

28 T. Morikita, T. Yamamoto, *J. Organomet. Chem.* 2001, **637**, 809.

29 X. S. Xu, X. Q. Li, H. Z. Gu, Z. B. Huang, X. H Yan, *Appl. Cata. A.* 2012, **429-430**, 17.

30 J. Zhang,; D. Shan, S. L Mu. *Polymer*. 2007, **140**, 1269.

31 L. Chaicharoenwimolkul, S. Chairam, M. Namkajorn, A. Khamthip, C. Kamonsatikul, U. Tewasekson, S. Jindabot, W. Pon-On, E. Somsook. *J. Appl. Polym. Sci*. 2013, **130**, 1489.

32 E. M. Geniés , P. Noël , *J. Electroanal. Chem.* 1990, **296**, 473.

33 M. K. Ram, S. Carrara, S. Paddeu, C. Nicolini, *Thin. Solid. Films.* 1997, **302**, 89.